



Yield Behavior of Solution Treated and Aged Ti-6Al-4V

Andrew J. Ring
Ohio Aerospace Institute, Brook Park, Ohio

Eric H. Baker
Connecticut Reserve Technologies, Inc., Cleveland, Ohio

Jonathan A. Salem and John C. Thesken
Glenn Research Center, Cleveland, Ohio

NASA STI Program . . . in Profile

Since its founding, NASA has been dedicated to the advancement of aeronautics and space science. The NASA Scientific and Technical Information (STI) program plays a key part in helping NASA maintain this important role.

The NASA STI Program operates under the auspices of the Agency Chief Information Officer. It collects, organizes, provides for archiving, and disseminates NASA's STI. The NASA STI program provides access to the NASA Aeronautics and Space Database and its public interface, the NASA Technical Reports Server, thus providing one of the largest collections of aeronautical and space science STI in the world. Results are published in both non-NASA channels and by NASA in the NASA STI Report Series, which includes the following report types:

- **TECHNICAL PUBLICATION.** Reports of completed research or a major significant phase of research that present the results of NASA programs and include extensive data or theoretical analysis. Includes compilations of significant scientific and technical data and information deemed to be of continuing reference value. NASA counterpart of peer-reviewed formal professional papers but has less stringent limitations on manuscript length and extent of graphic presentations.
- **TECHNICAL MEMORANDUM.** Scientific and technical findings that are preliminary or of specialized interest, e.g., quick release reports, working papers, and bibliographies that contain minimal annotation. Does not contain extensive analysis.
- **CONTRACTOR REPORT.** Scientific and technical findings by NASA-sponsored contractors and grantees.

- **CONFERENCE PUBLICATION.** Collected papers from scientific and technical conferences, symposia, seminars, or other meetings sponsored or cosponsored by NASA.
- **SPECIAL PUBLICATION.** Scientific, technical, or historical information from NASA programs, projects, and missions, often concerned with subjects having substantial public interest.
- **TECHNICAL TRANSLATION.** English-language translations of foreign scientific and technical material pertinent to NASA's mission.

Specialized services also include creating custom thesauri, building customized databases, organizing and publishing research results.

For more information about the NASA STI program, see the following:

- Access the NASA STI program home page at <http://www.sti.nasa.gov>
- E-mail your question to help@sti.nasa.gov
- Fax your question to the NASA STI Information Desk at 443-757-5803
- Phone the NASA STI Information Desk at 443-757-5802
- Write to:
STI Information Desk
NASA Center for AeroSpace Information
7115 Standard Drive
Hanover, MD 21076-1320



Yield Behavior of Solution Treated and Aged Ti-6Al-4V

Andrew J. Ring
Ohio Aerospace Institute, Brook Park, Ohio

Eric H. Baker
Connecticut Reserve Technologies, Inc., Cleveland, Ohio

Jonathan A. Salem and John C. Thesken
Glenn Research Center, Cleveland, Ohio

National Aeronautics and
Space Administration

Glenn Research Center
Cleveland, Ohio 44135

Acknowledgments

The authors thank Joe Lewis, NASA Jet Propulsion Laboratory (JPL) for valuable input and comments on the testing and results.

Level of Review: This material has been technically reviewed by technical management.

Available from

NASA Center for Aerospace Information
7115 Standard Drive
Hanover, MD 21076-1320

National Technical Information Service
5301 Shawnee Road
Alexandria, VA 22312

Available electronically at <http://www.sti.nasa.gov>

Yield Behavior of Solution Treated and Aged Ti-6Al-4V

Andrew J. Ring
Ohio Aerospace Institute
Brook Park, Ohio 44142

Eric H. Baker
Connecticut Reserve Technologies, Inc.
Cleveland, Ohio 44040

Jonathan A. Salem and John C. Thesken
National Aeronautics and Space Administration
Glenn Research Center
Cleveland, Ohio 44135

Summary

Post yield uniaxial tension-compression tests were run on a solution treated and aged (STA), titanium 6-percent aluminum 4-percent vanadium (Ti-6Al-4V) alloy to determine the yield behavior on load reversal. The material exhibits plastic behavior almost immediately on load reversal implying a strong Bauschinger effect. The resultant stress-strain data was compared to a 1D mechanics model and a finite element model used to design a composite overwrapped pressure vessel (COPV). Although the models and experimental data compare well for the initial loading and unloading in the tensile regime, agreement is lost in the compressive regime due to the Bauschinger effect and the assumption of perfect plasticity. The test data presented here are being used to develop more accurate cyclic hardening constitutive models for future finite element design analysis of COPVs.

Introduction

Monolithic metallic propellant tanks have been used in a variety of space-related missions such as the Space Shuttle, the International Space Station, and the Apollo missions. The stresses in these tanks were always elastic. Such tanks can be made lighter and more reliable than the metallic counterparts by overwrapping a metallic liner with epoxy impregnated fibers such as Kevlar or carbon, and shedding much of the load to the relatively strong fibers. In such composite overwrapped pressure vessels, the metallic liner is usually yielded due to an initial autofrettage process, but still shares some of the load with the dominant composite overwrap. In order to further reduce the mass of spacecraft propellant tanks, ultra-thin liners that bear little load but act as a compatibility and gas barrier are being developed for missions such as the Europa Clipper, the Mars Skycrane, and the Mars 2020 mission.

Design of COPVs using ultra-thin metallic liners requires an understanding of the fully reversed, plastic behavior of the liner material, and mechanics models that match the material behavior. In this work, the uniaxial tensile behavior of a solution treated and aged Ti-6Al-4V alloy was determined in strain control and compared to the expected, analytically derived COPV response.

Theoretical Considerations and Analysis of the Mars 2020 COPV

1D Mechanics Model

The stress-strain histories applied to the test specimens were derived from the expected response of the Mars 2020 COPV. Thus a brief overview of the fundamental behavior of metal liner COPVs is given. The COPV mechanical response follows from a 1D closed-form representation of the major hoop-oriented principal strain. For cylindrical vessels, hoop strain is often the dominant fiber and liner strain

unless there are specific geometric details causing stress and strain concentrations. Early forms of this theoretical development are given in References 1 and 2, and a recent NESC report Reference 3 demonstrates the value of these methods for interpreting COPV test data and providing accurate bounds of the maximum hoop strains.

The COPV hoop strain is usually graphed on the vertical axis as a function of vessel pressure on the horizontal axis as done schematically in Figure 1(a). Strain continuity is assumed between a linear-elastic overwrap and a linear-elastic, perfectly-plastic (PP) liner. The resultant, individual strain-stress curves are shown in Figures 1(b) and (c) for correlation of common strain points. The bi-linear vessel strain-pressure response for the initial autofrettage cycle to proof pressure is shown as two intersecting green lines in Figure 1(a). The post-autofrettage unloading and all future operational loads trace the blue line. The residual tensile strain in the overwrap is represented by the offset of the blue line at the origin when pressure returns to zero.

The adjacent, composite overwrap strain-stress response is assumed to be linear-elastic, as shown by the yellow strain-stress curve in Figure 1(b). The corresponding liner strain-stress response is assumed to be linear-elastic, perfectly-plastic (PP) with green and blue lines corresponding to the vessel autofrettage and operating response, respectively. Note that above the liner yield point, the perfectly-plastic liner carries no further load so its plastic strain is controlled by the deformation of the composite. The accumulated plastic strain becomes an interference strain between the overwrap and liner. Post autofrettage, the blue unloading line for the liner material reveals that a portion of the interference strain is shared by the liner as a residual compressive stress that balances the residual tensile stress in the composite. Subsequent loads to burst retrace the operating blue line to reinitiate yield at the former autofrettage pressure; the path to burst above autofrettage is shown as red line segments in the vessel and liner response curves.

If the liner had been simulated using a cyclic hardening constitutive model, it would be possible to initiate reverse yielding at a lower flow stress and allow relaxation of the residual stresses, thereby mimicking the Bauschinger effect.

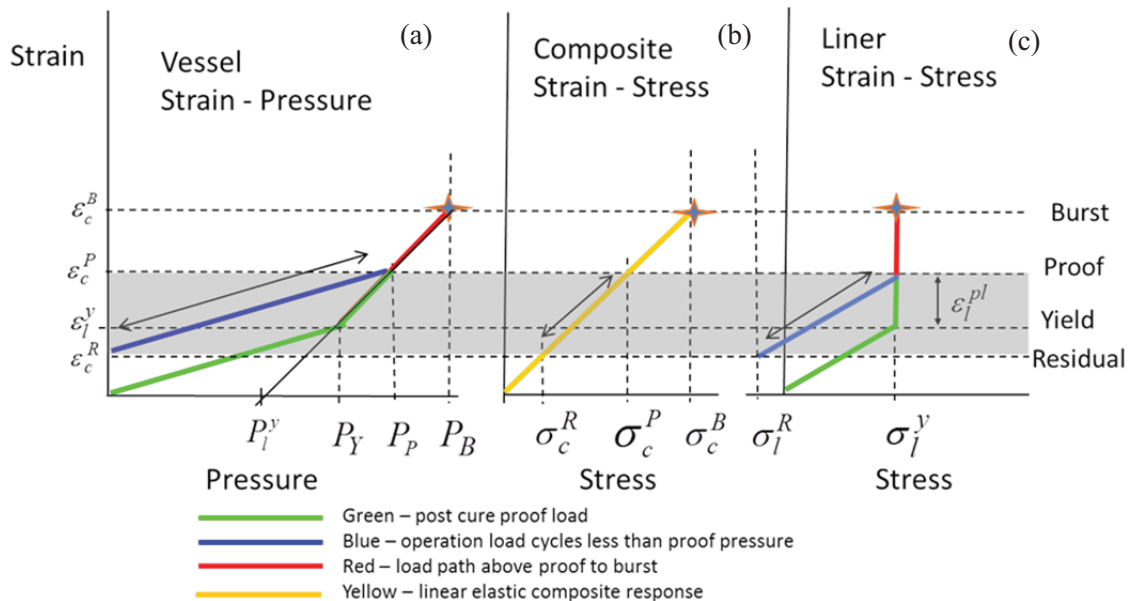


Figure 1.—Composite pressure vessel strain-pressure response correlated with composite and liner strain-stress responses assuming continuity between vessel constituents, a linear-elastic composite overwrap, and a linear-elastic, perfectly-plastic liner: (a) Vessel strain-pressure, (b) Composite strain-stress, and (c) Liner strain-stress. The vessel reflects a piece-wise linear response due to the combined effects of the liner and the composite overwrap. The green lines represent the vessel response post cure due to autofrettage to proof pressure. Subsequent unload and reload to operating pressures less than or equal to proof follow the blue lines and produce strains within the shaded region of the curve.

Finite Element Analysis

Besides a 1D mechanics approach, the Mars 2020 COPV has been modeled (by the COPV vendor) using ABAQUS based Finite Element Analysis (FEA). Figure 2 shows a swept segment of the FEA model developed by the COPV vendor. Colors in Figure 2(a) represent the various material properties where the range of colors in the dome region represents the changing material properties as a function of changing fiber wind angle in the vessel dome. The solid colors in the cylinder (red) and skirt (blue) represent a uniform fiber angle in those regions. Figure 2(b) shows the hoop strain distribution in the vessel at burst pressure.

The liner hoop stress-strain response and equivalent stress-strain response from the Mars COPV finite element analysis are shown in Figure 3(a) and (b), respectively. The hoop stress-strain response from the finite element analysis results are quite similar to but discernable from the 1D elastic perfectly-plastic representation of the liner constitutive response shown in Figure 1(c). The initial load to autofrettage pressure (0-AF) cycle traces the initial yield of the liner to about 1.2 percent hoop strain. The unload pressure cycle (AF-0) shows that the liner behaves linear elastically down to $-50,000$ psi as there is no reverse yielding of the liner in compression with the removal of pressure. Subsequent loading cycles do not appear to reinitiate liner yield until the prior AF pressure is exceeded at 1.2 percent strain during the MDP-Burst cycle enroute to vessel burst at a hoop strain above 1.4 percent.

The equivalent stress-strain curve provides a complete representation of the multi-axial stress-strain response in scalar form. The equivalent stress-strain response includes not only the axial and radial normal stresses and strains, but the shear stresses and strains in the radial-axial plane induced by the geometric asymmetry of this vessel. These additional contributions result in a uniaxial equivalent strain of 1.6 percent at AF, making a discernable difference between the 1D and FEA approaches. Note that equivalent stress is always positive even though the liner is in compression during unloading. Without cyclic hardening effects in this constitutive model, there is no Bauschinger effect occurring during the unload; additional load cycles will retrace this unloading curve as long as the peak load remains less than the peak load at AF.

In order to understand the significance of the model's limitations, tensile tests were designed to explore the reversed load response of the liner. The tests and results are discussed in the following sections.

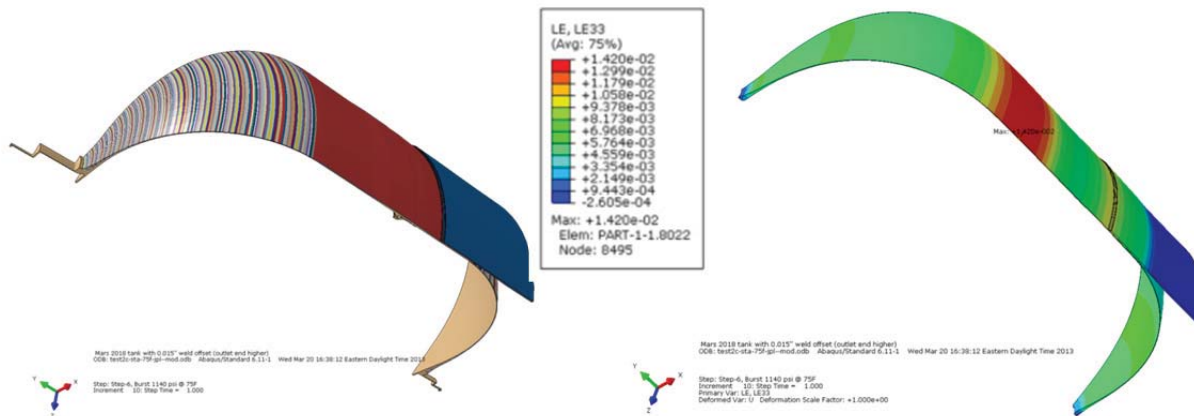


Figure 2.—(a) ABAQUS Finite Element Model of the Mars 2020 COPV with color coded material properties, and (b) Hoop strain distribution at burst pressure.

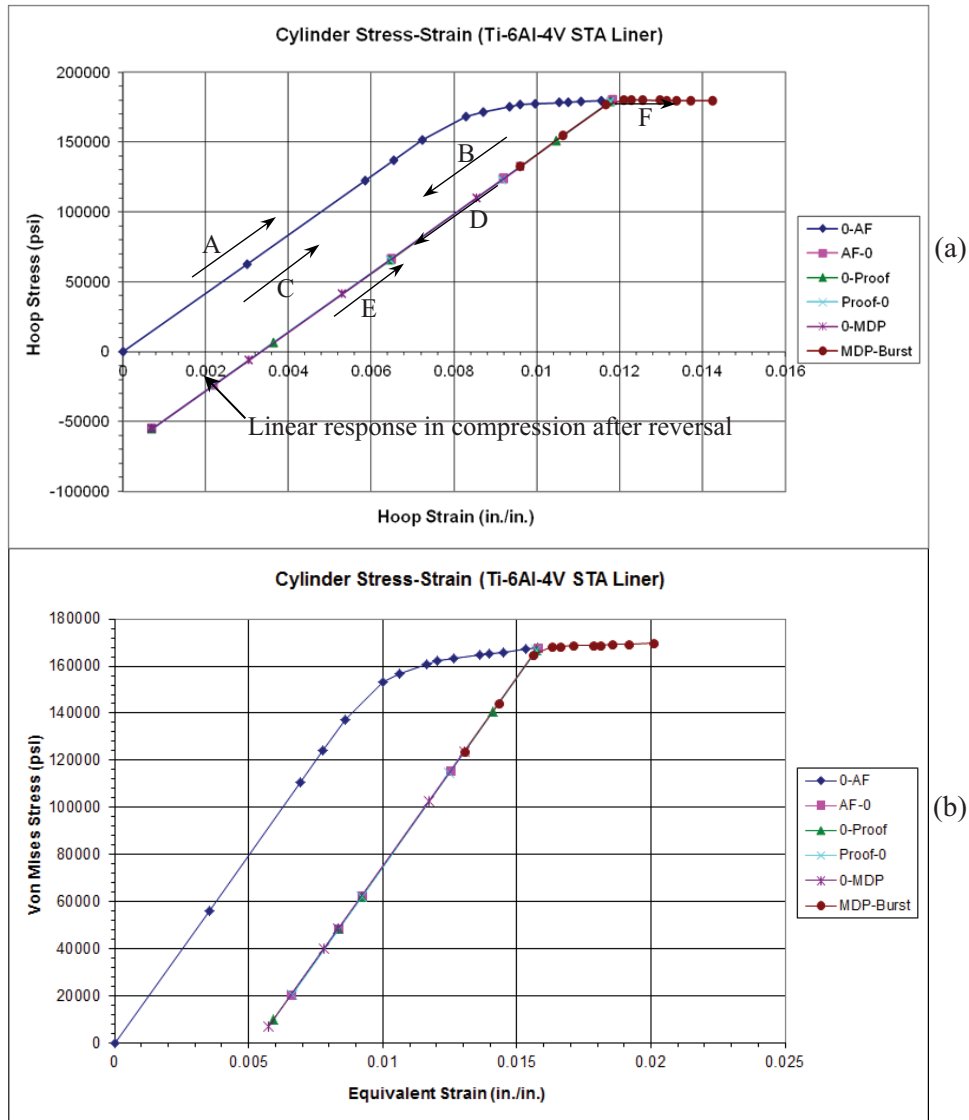


Figure 3.—Pressure cycle induced (a) hoop stress-strain response and (b) uniaxial equivalent stress-strain response via COPV FEA.

Experimental Procedure

Eight ASTM E8 subsize sheet-type specimens (Ref. 1) were extracted from a Ti-6Al-4V (STA) forging that was processed per AMS 81200 and proprietary specifications. Uniaxial tension-compression tests were performed by loading in strain control. A 1-in. gage length extensometer was used to control the test at a strain rate of 830 microstrain per second. Four of the specimens were subjected to a specific load history in order to simulate potential autofrettage, proof, and maximum design pressure (MDP) cycles:

TL-1—The specimen was loaded in tension to 1.6 percent strain followed by compression of -2 percent from the zero-load strain value. The specimen was then loaded in tension to a proof stress of 167 ksi and unloaded.

TL-2—Loaded in tension to 1.6 percent strain and unloaded. The specimen was then subjected to five compression-tension cycles of -55.4 to 150 ksi.

TL-3—Loaded in tension to 1.6 percent strain and unloaded. The specimen was then subjected to two compression–tension cycles between –55.3 and 166.7 ksi, and unloaded. Next, two cycles of compression to –55.3 ksi with tension to 127.8 ksi followed by unloading were performed. Finally, the specimen was compressed to –55.3 ksi and then loaded monotonically in tension to failure. To ensure the strain-to-failure would not exceed the 10 percent strain range of the extensometer, the control mode was switched to stroke upon the final load reversal. A stroke rate of 0.00296 in./sec was set in an attempt to approximate the 830 microstrain per second strain rate used during the rest of the test.

TL-4—Identical to the loading of TL-3 except for the strain rate during loading to failure: After 6 percent strain the control mode was switched to stroke at a rate of 0.00095 in./sec to better approximate a strain rate of 830 microstrain per second.

In order to determine the effect of the various load cycles on tensile strength properties, an additional test (specimen TL-7) was run per ASTM E8.

Experimental Results

Figures 4 to 7 show the measured stress-strain curves corresponding to the load histories described previously. As with annealed Ti-6Al-4V (Ref. 3), solution treated and aged material clearly exhibits a Bauschinger effect with nonlinear behavior occurring almost immediately upon load reversal. The loops are fairly stable and the strain curve continues to failure almost contiguously: only a 15 ksi increase in stress is required to continue extension, as shown in Figures 6 and 7. Table 1 summarizes tensile properties derived from the test specimen measurements. It should be noted that Young’s modulus and the yield strength were determined from the initial loading in the usual way (Ref. 4), however, the reported ultimate and break strengths for cases TL-3 and TL-4 were determined after multiple load cycles. Despite the load cycles, the results are similar to Ti-6Al-4V STA tested monotonically per ASTM E8, shown in Figure 8 and Table 1.

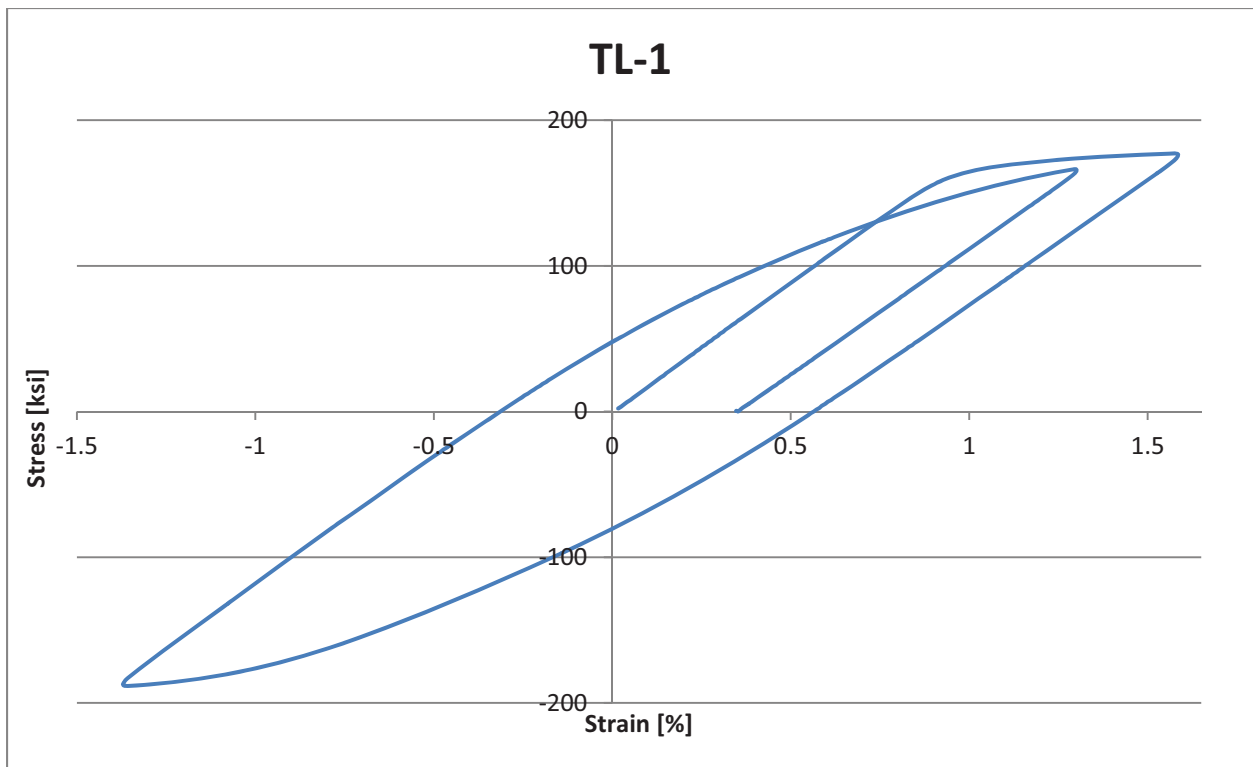


Figure 4.—Stress-strain history for specimen TL-1.

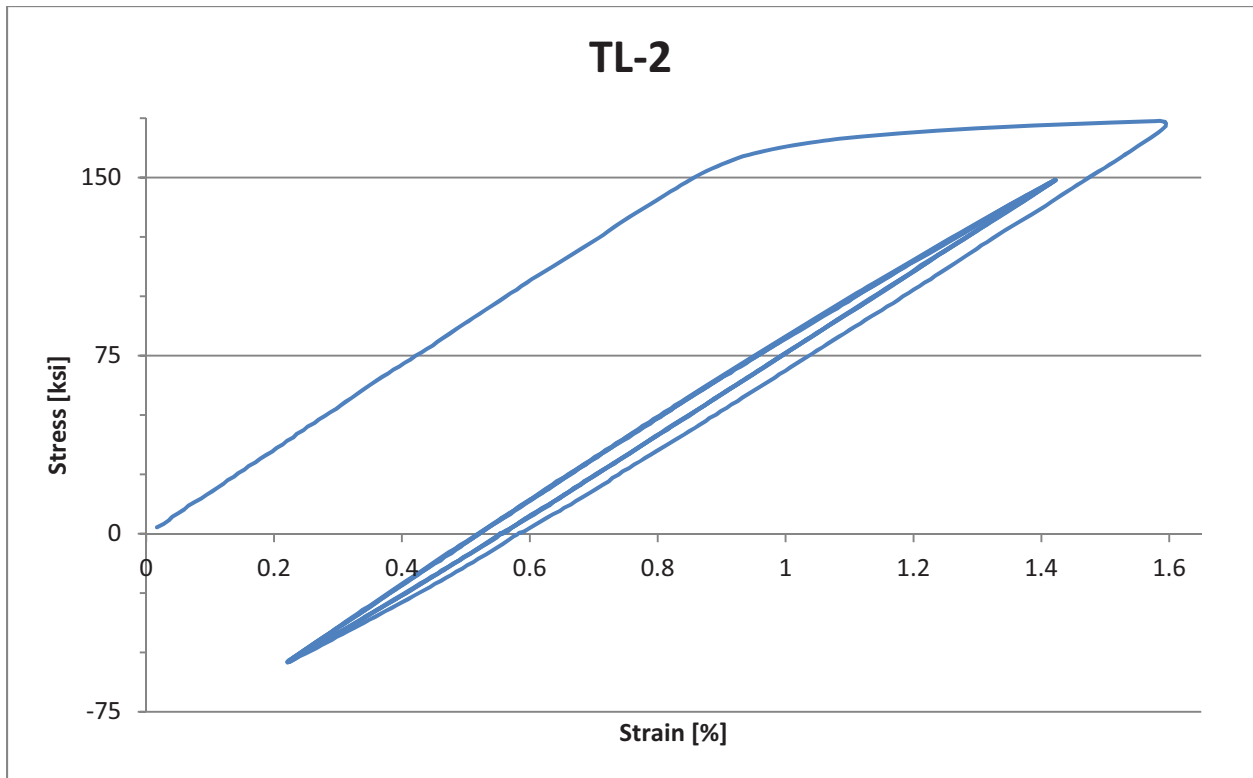


Figure 5.—Stress-strain history for specimen TL-2.

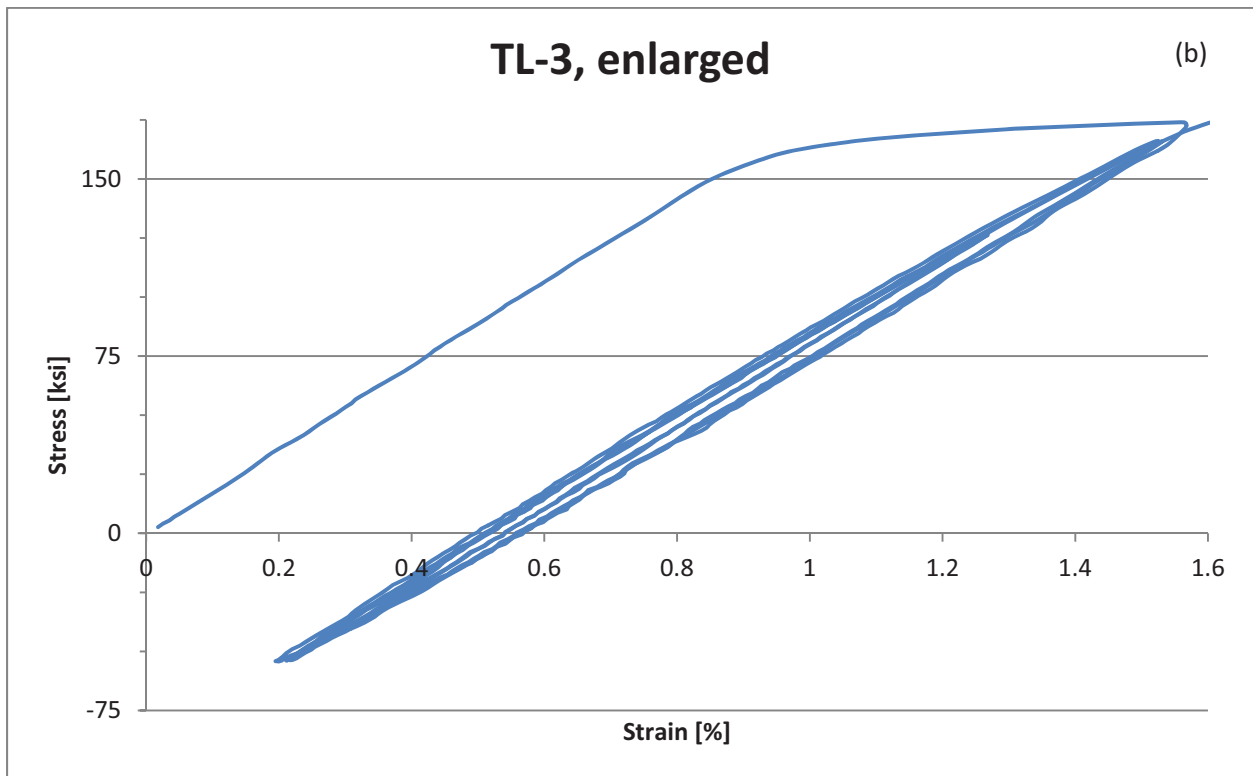
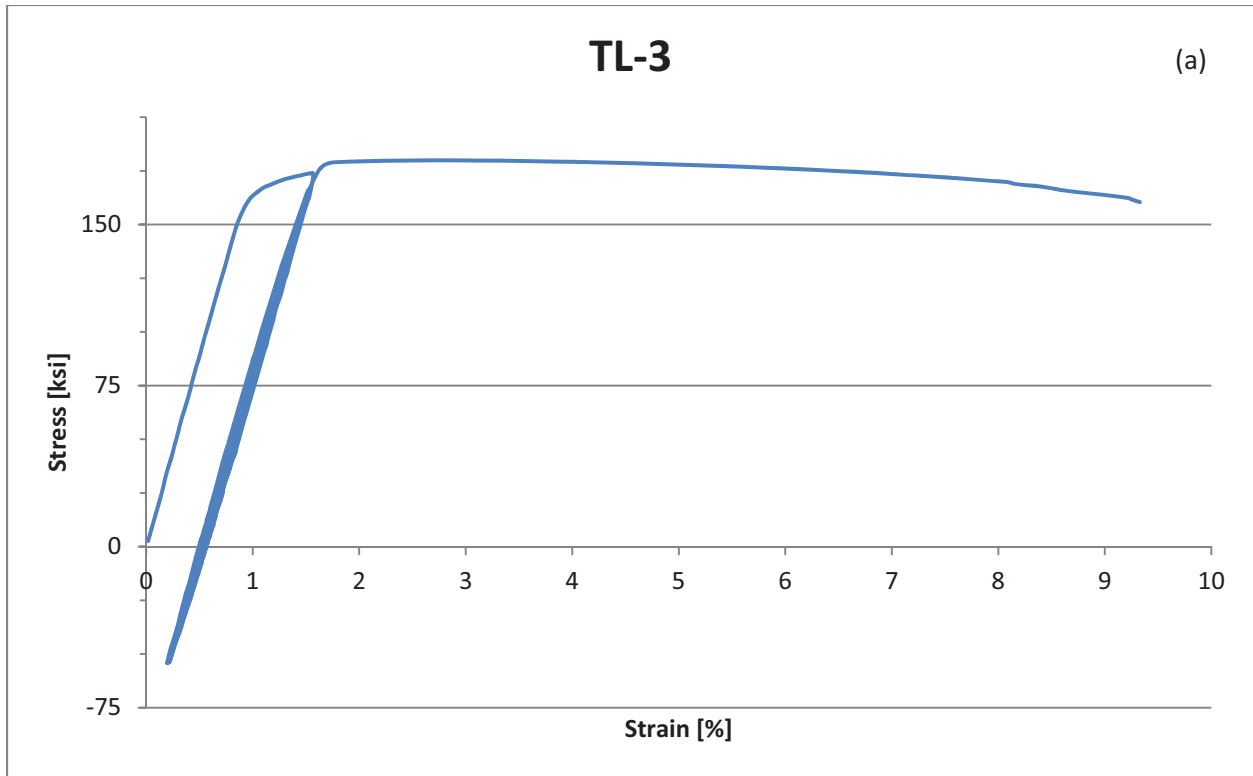


Figure 6.—(a) Stress-strain history for specimen TL-3; (b) Enlarged view of the cyclic portion.

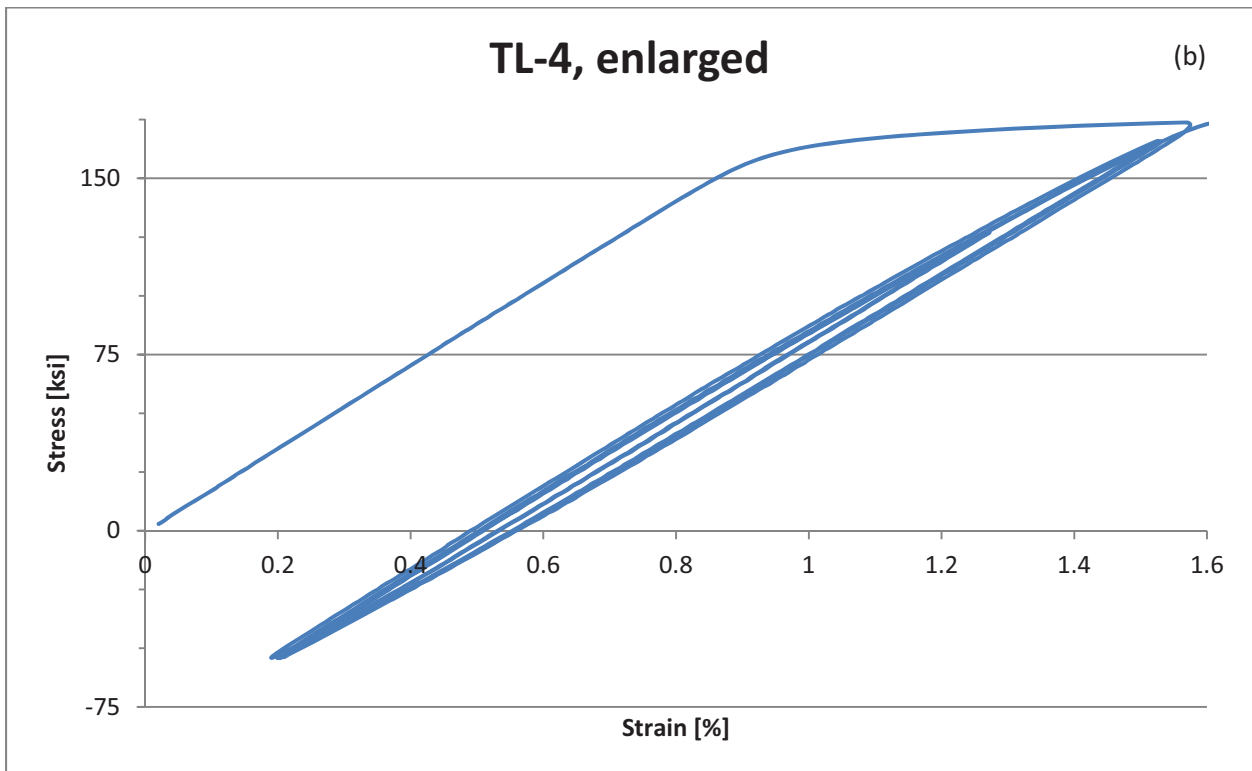
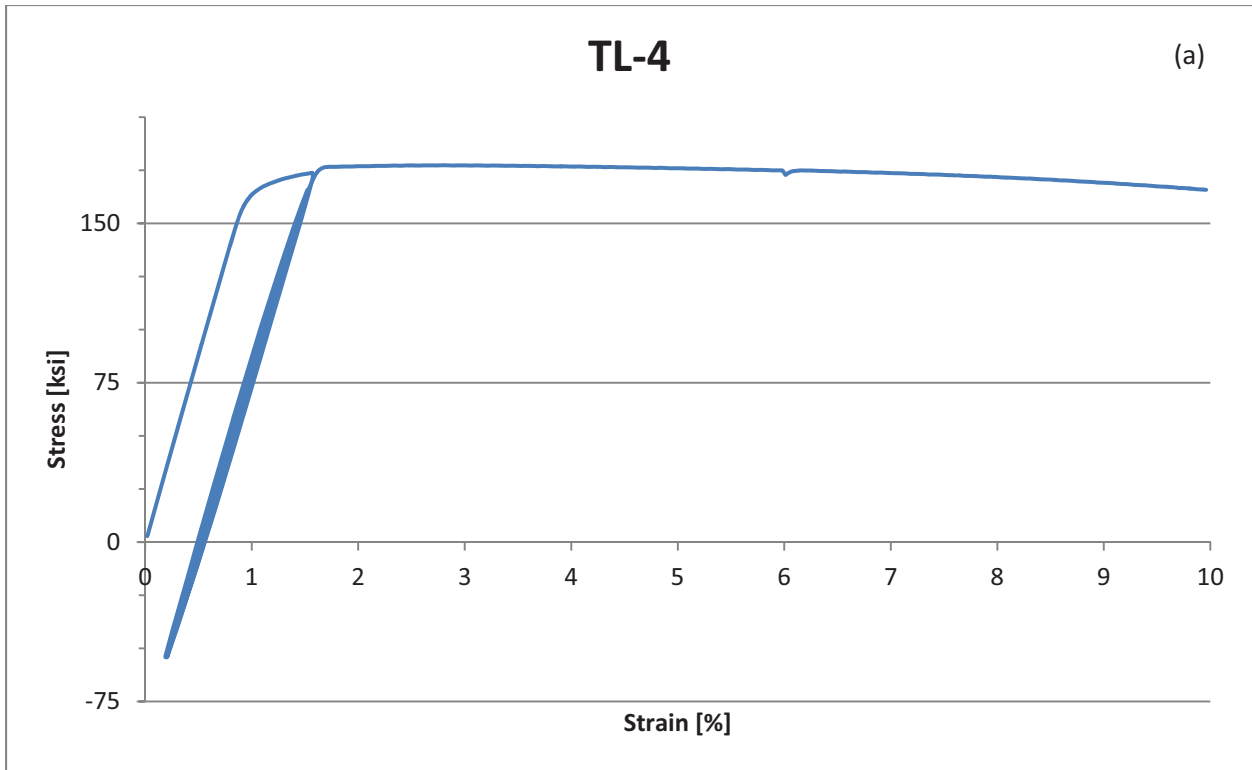


Figure 7.—(a) Stress-strain history for specimen TL-4; (b) Enlarged view of cyclic portion.

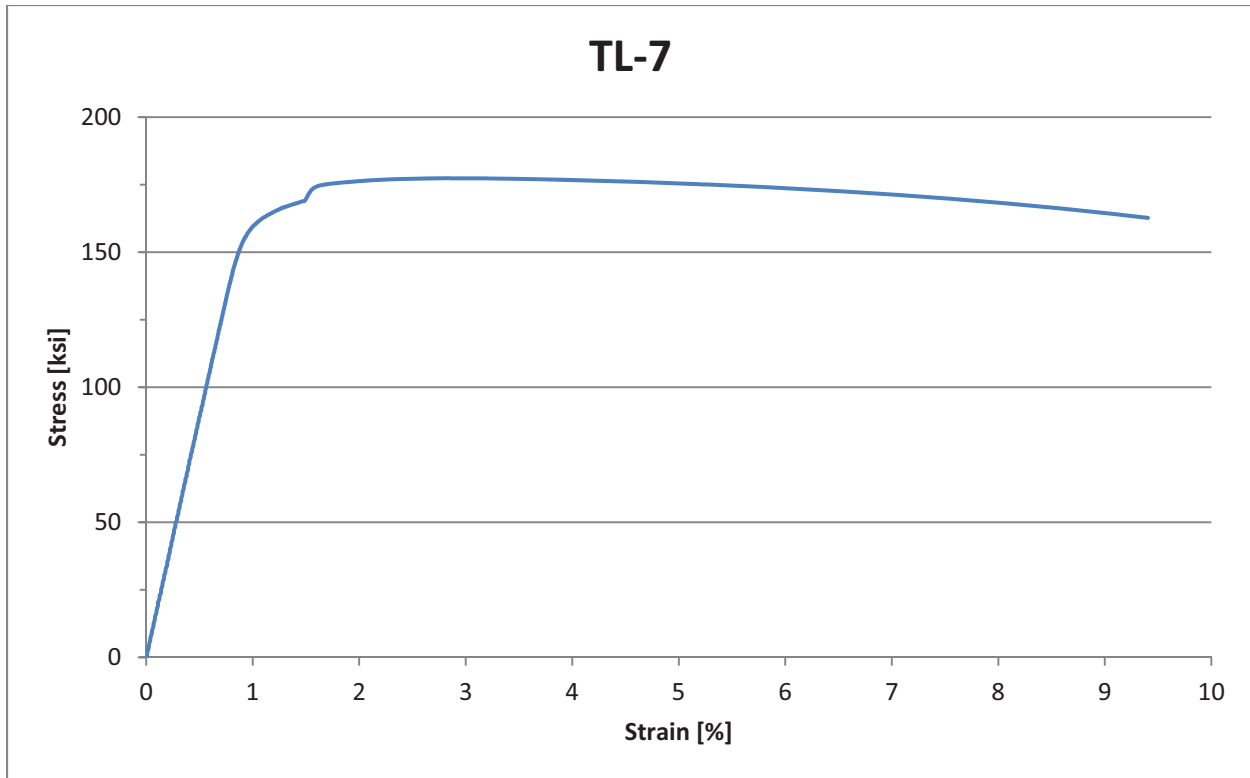


Figure 8.—Stress-strain history for specimen TL-7.

TABLE 1.—TENSILE PROPERTIES

Specimen number	Young's modulus, Msi	Yield strength, ksi	Maximum stress, ksi	Break stress, ksi	Elongation, percent
TL-1	17.4	167	----	----	----
TL-2	17.4	165	----	----	----
TL-3	17.5	165	176	157	9.7
TL-4	17.2	165	173	154	12.4
TL-7 (Monotonic per E8)	17.3	160	174	150	10.8

Discussion of Results and Correlation With FEA Analysis

Further insight into measured stress-strain responses can be gained by recasting the results in terms of stress as a function of either elastic strain or plastic strains. These forms of the experimental results clarify when plastic strain is changing, and can be used to separate elastic strain energy from the dissipated plastic work. Having the experimental data in this format is often preferred when deriving constitutive models for computational analysis. Typically, the separation is achieved by deriving the effective elastic modulus from the stress-strain data, computing the elastic strain for each stress data point, and subtracting that elastic strain from the total strain to determine the plastic strain corresponding to that data point. An example is given in Figure 9 where the results from test TL-1 (blue) are shown along with the stress-elastic strains (magenta) and stress-plastic strains (green). The vertical green lines represent the segments of the load cycle where plastic strains are not changing, generally at the beginning of each new load segment. The Bauschinger effect is clearly seen during the first unload cycle as stress changes from tensile to compression and plastic strain reverses immediately. Recall no such nonlinear response was present in the FEA representation of the vessel response (see arrow in Fig. 3(a)).

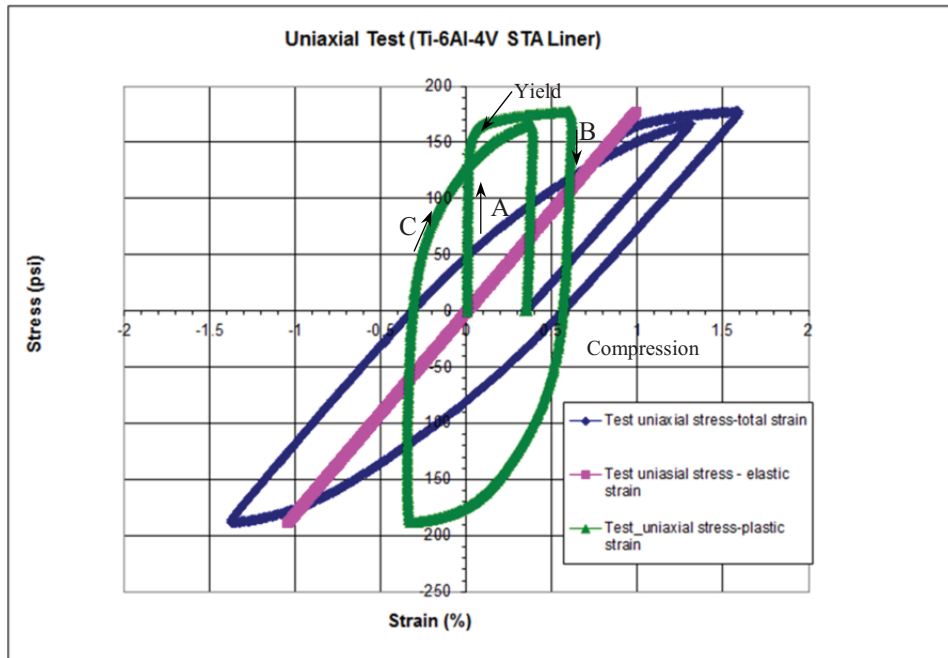


Figure 9.—The stress-strain response shown from case TL-1 separated into stress-elastic strain and stress-plastic strain curves to clearly show changes in plastic strain due to reverse yielding during unloading and reloading.

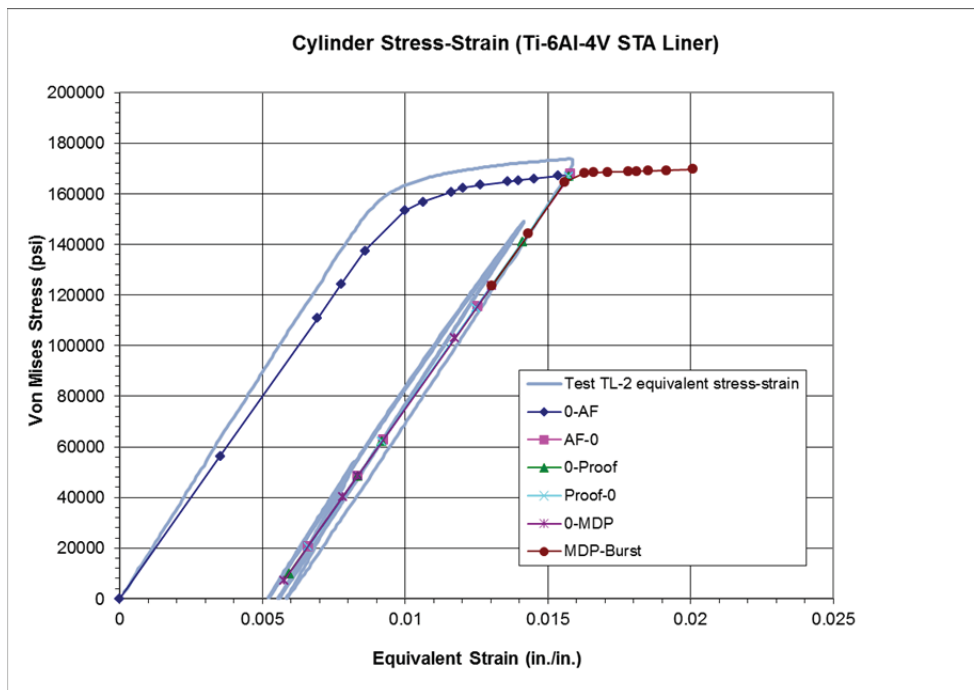


Figure 10.—Comparison of the measured and predicted uniaxial equivalent stress-strain results for the Mars 2020 COPV.

Direct correlation of the uniaxial results with the FEA results can be made by computing the equivalent stress-strain response from the experimental data and co-plotting with the equivalent stress-strain response of the vessel. This is shown for TL-2 in Figure 10 where the red curve represents the experimental data and the underlying segment curve with data points is the same equivalent stress-strain curve shown in Figure 3(b).

The uniaxial test specimen equivalent stress-strain response (red) in Figure 10 indicates a slightly greater elastic modulus during the initial loading than was used in the FEA model. The uniaxial yield stress is also slightly greater. Despite these modeling input differences, strain control during the uniaxial test matched the unload portion of the FEA response curve closely until zero stress is reached.

The uniaxial test specimen response clearly changes to a nonlinear trajectory while passing through zero stress as the specimen goes into compression (Figs. 4 and 9). Thus negative strains occur. The pressure vessel liner, however, is predicted to experience only linear behavior. Note that the inflection points in the equivalent stress-strain plot of the experimental data that occur are associated with strain sign changes and also when unloading begins from maximum compression stress. The nonlinear portion of the uniaxial unload-reload trace would have collapsed to the FEA unload-reload line if the plastic strain had remained constant and there were no Bauschinger effect present in the measured data.

Conclusion

Tensile tests run in order to simulate the behavior of ultra-thin liners in light-weight composite overwrap pressure vessels imply a Bauschinger effect and immediate nonlinearity upon load reversal. The tensile properties after several load reversals were similar to those determined monotonically.

Mass-efficient COPVs using ultra-thin Ti-6Al-4V STA liners cannot be designed to have elastically responding liners but must be designed with plastically responding liners.

Comparison of experiments and models implies reasonable agreement until compressive stresses are induced into the liner. As demonstrated by the experimental results, an elastic perfectly-plastic analysis is inadequate to estimate liner stress and strain states. Strain hardening, as experimentally measured herein, needs to be incorporated in future COPV models.

References

1. Thesken, J. NASA/TM—2009-215683, Composite Overwrap Pressure Vessels: Mechanics and Stress Rupture Lifting Philosophy.
2. Thesken, J. NASA/TM—2009-215684, A Theoretical Investigation of Composite Overwrap Pressure Vessels (COPV) Mechanics Applied to NASA Full Scale Tests.
3. NESC CPVWG Task 4: A Theoretical and Experimental Investigation of COPV Autofrettage, NASA Engineering and Safety Center Technical Assessment Report, NESC-RP-09-00537, Dec 2013.
4. ASTM E8, in Annual Book of Standards, volume 03.01, American Society for Testing and Materials, W. Conshohocken, Pennsylvania (2003).
5. SAE AMS-H-81200-2001, Heat treatment of titanium and titanium alloys, SAE International, Warrendale, PA.
6. J.A. Salem, B. Lerch, J.C. Thesken, J. Sutter and R. Russell, “Strength, Fatigue and Fracture Toughness of Ti-6Al-4V Liner from a Composite Over-Wrapped Pressure Vessel,” NASA/TM—2008-215147, March 2008.

